Finite Larmor radius effects and velocity correlations in two-dimensional electrostatic plasma turbulence

B. Krane and H. L. Pécseli
University of Oslo, Institute of Physics, Box 1048 Blindern, N-0316 Oslo, Norway

J. Trulsen
University of Oslo, Institute of Theoretical Astrophysics, Box 1029 Blindern, N-0315 Oslo, Norway
(Received13 May 1996)

Low-frequency electrostatic turbulence in low-β plasmas is studied in two spatial dimensions by direct numerical simulations. In this limit the guiding center velocity in the direction perpendicular to a homogeneous magnetic field is in a first approximation the $\boldsymbol{E}\times\boldsymbol{B}_0/B_0^2$ velocity. The electron Larmor radius can safely be set to zero for most relevant conditions, but the ion dynamics are noticeably influenced by their finite Larmor radius. In the present study we use a fluid model where these effects are included by a simple filtering operation. The equilibrium spectra are investigated and compared with known analytical results. Particular attention is given to the finite Larmor radius effect for the turbulent diffusion of charged particles across magnetic field lines. The integral time scale and the micro time scale associated with the velocity correlations for the turbulent flow are discussed with attention to their dependence on the finite Larmor radius corrections. Finally, the numerical code is generalized to a hybrid model, which incorporates many ion species with different Larmor radii simultaneously present in the flow. [S1063-651X(97)00601-6]

PACS number(s): 52.65.−y, 52.25.Gj

I. INTRODUCTION

Low-frequency electrostatic turbulence in strongly magnetized plasmas allows the analysis to be carried out in two dimensions in the limit where magnetic field lines can be considered equipotential, and the magnetic field assumed homogeneous. Then the local plasma velocity can be approximated by $\boldsymbol{v}=-\nabla\Phi\times\boldsymbol{B}_0/B_0^2$, provided characteristic frequencies are well below the ion gyro frequency Ω_{ci}. The equation of continuity for electrons and ions then becomes the Euler equation

$$\frac{\partial n_{e,i}(\boldsymbol{r},t)}{\partial t}+\frac{1}{B_0}[\Phi(\boldsymbol{r},t),n_{e,i}(\mathbf{r},t)]=0, \tag{1}$$

where [,] denotes Poisson brackets and the electrostatic potential Φ takes the role of the stream function. Together with Poisson's equation

$$\nabla^2\Phi(\boldsymbol{r},t)=-\frac{e}{\varepsilon_0}[n_i(\boldsymbol{r},t)-n_e(\boldsymbol{r},t)], \tag{2}$$

a closed, standard equation is obtained for Φ,

$$\frac{\partial}{\partial t}(\nabla^2\Phi)-[(\nabla\Phi\times\boldsymbol{b})\cdot\nabla]\nabla^2\Phi=0. \tag{3}$$

The equation is written in dimensionless form and the correct length, time, and potential are found by multiplying with r_0, $t_0=\omega_{ci}/\omega_{pi}^2$, and $\Phi_0=n_0er_0^2/\epsilon_0$, respectively. Here r_0 is a scale length characterizing the initial condition. Since there is no characteristic spatial scale length in the equations, the turbulence for the zero Larmor radius model is scale invariant. This model has been extensively investigated, for instance, by Seyler *et al.* [1], and a review of its implications to ionospheric turbulence is discussed by Kintner and Seyler [2].

Equations (1) and (2) assume that the positions of the charged particles are well approximated by their guiding centers. For electrons this is valid for most physically relevant cases, but the assumption might fail for the ions due to their larger Larmor radii. A straightforward, but computationally costly, remedy assumes a full gyrating particle description. A standard fluid model, where the finite Larmor radius (FLR) effects are introduced through the gyro viscosity, was derived by Braginskii [3]. Recently this analysis has been extended by Smolyakov *et al.* [4].

A simpler fluid model includes the lowest order FLR effects by introducing an operator acting on the electric field [5]. By this the averaging of the electric field along the circular gyro orbit of an ion with gyro radius ρ is approximated, with the assumption that the characteristic length scale for the electric field variations is much larger than ρ. The resulting ion gyro center velocity is obtained as

$$\boldsymbol{v}_i=\left(1+\frac{1}{4}\rho^2\nabla^2\right)\boldsymbol{E}\times\boldsymbol{B}_0/B_0^2. \tag{4}$$

The effective ion $\boldsymbol{E}\times\boldsymbol{B}$ velocity thus differs from that of the electrons, i.e., the ion mobility differs from the electron mobility due to FLR effects. The model (4) has been discussed, e.g., by Stasiewicz [6] in the case of large Larmor radius effects in the magnetosphere. When polarization drifts are ignored this approximation is formally adequate, but it is incorrectly weighting short scale length fluctuations. Even if their amplitude is by assumption small, this weighting is numerically unfavorable. An alternative and numerically more robust model was suggested by Knorr *et al.* [7], where a fluid model is formally retained, but the averaging along the ion

orbit is carried out accurate to all orders. Also the modification of ion density is included since the ion density differs from the guiding center density when FLR corrections are included; a modification of the effective ion drift alone is insufficient and gives an inconsistent model. The resulting numerical scheme is easy to implement and is only slightly more time consuming than the solution of (4). Analytical results are available for the model which can serve as nontrivial tests of the code.

The paper is organized as follows. In Sec. II the model and its applicability are discussed, both for a two-fluid and a multi-ion fluid model. In Sec. III an outline of the numerical implementation is given. Analytical expressions for the asymptotic state of the two-fluid model is compared to results from direct numerical simulations in Sec. IV. Next, in Sec. V the dispersion of passive test particles and the corresponding time scales are presented for a systematic variation of the ion Larmor radius. Finally, our results are summarized in section VI.

II. FLR CORRECTIONS TO ARBITRARY ORDER

A computationally preferable alternative to (4) is to retain the full expression from the averaging of the electric field over the gyro orbit. As previously discussed, the electric field experienced by a gyrating charged particle is no longer the same as the electric field evaluated at the guiding center. Knorr *et al.* [7] derived an expression for the corrected guiding center velocity, indicated by an overbar,

$$\overline{\boldsymbol{v}}(\boldsymbol{x})=\sum_{\boldsymbol{k}} J_0(k\rho)\boldsymbol{v}_{\boldsymbol{k}} \exp(i\boldsymbol{k}\cdot\boldsymbol{x}), \tag{5}$$

where the vector component $\boldsymbol{v}_{\boldsymbol{k}}$, without the overbar, is obtained from the $\boldsymbol{E}\times\boldsymbol{B}$ velocity evaluated at the guiding center. J_0 is the Bessel function of order zero. The polarization drift is ignored, imposing restrictions on the applicability of the model [7]. The relative magnitude of the polarization drift as compared to the $\boldsymbol{E}\times\boldsymbol{B}$ drift is in a first approximation $\langle\omega\rangle/\omega_{ci}$, where the characteristic frequency $\langle\omega\rangle$ is to be obtained along the particle trajectory. As an estimate we have $\langle\omega\rangle\sim kv_{\rm th}$ in terms of the thermal velocity and wave number, giving $\langle\omega\rangle/\omega_{ci}\sim k\rho$. The polarization drift may be ignored for small $k\rho$ in strongly magnetized plasmas. The latter requirement implies $\omega_{pi}^2\ll\omega_{ci}^2$ in the low-frequency relative dielectric constant $\epsilon_\perp=1+\omega_{pi}^2/\omega_{ci}^2$. Note that the FLR-corrected flow remains incompressible, just as the $\boldsymbol{E}\times\boldsymbol{B}$ flow.

A series expansion of $J_0(k\rho)$, assuming $k\rho\ll 1$, gives $J_0(k\rho)\approx 1-\frac{1}{4}(k\rho)^2$. Retaining only the leading terms, we obtain the standard [5] correction to the guiding center velocity as given by Eq. (4). From the series expansion we note that FLR corrections correspond to a reduction in magnitude of the guiding center velocity for a harmonically varying electric field. The governing equations remain well behaved for all ρ, in particular also in the limit $\rho\to\infty$ since $J_0(k\rho\to\infty)=0$. It should be emphasized, however, that this limit is inconsistent with the basic physical assumptions underlying the expression for the guiding center drift.

The effective, or corrected, guiding center velocity discussed in this paper is distinct from the velocity appearing in the usual fluid equations; in that case the velocity is the average of all particle velocity vectors crossing a small reference area.

Also the ion density has to be corrected for FLR effects. Describing the dynamics of a magnetized, low-β plasma on a plane perpendicular to the magnetic field, the perturbations are assumed to be strictly $\boldsymbol{B}$-field aligned. The guiding centers of electrons and ions are then assumed to be uniformly distributed along magnetic field lines, and the phase angles in the gyration to be uniformly distributed in the interval $[0,2\pi\rangle$. The projection of the particle positions on the plane of analysis is then uniformly distributed on a circle for particles with given Larmor radius and gyro centers on a given magnetic field line. The analysis is similar to that giving the corrections to the $\boldsymbol{E}\times\boldsymbol{B}$ velocity [7] and the result is

$$\overline{n(\boldsymbol{x})}=\sum_{\boldsymbol{k}} J_0(k\rho)n_{\boldsymbol{k}} \exp(i\boldsymbol{k}\cdot\boldsymbol{x}). \tag{6}$$

From a prescribed guiding center density $n(\boldsymbol{x})$ we now calculate the corresponding charge density by filtering the Fourier coefficients of $n(\boldsymbol{x})$ with $g_{\boldsymbol{k}}=J_0(k\rho)$, or alternatively, by performing the appropriate convolution in configuration space.

Physically, the inclusion of FLR corrections consists of the following steps; first the Poisson equation is solved to give the electric field. Then the *effective* electric field is determined, corresponding to the appropriate Larmor radius for the given particle species. The particle *guiding centers* are moved in response to this effective field, with the density of the appropriate guiding centers following a continuity equation. Then the electric field is again obtained from Poisson's equation, where the local electron and ion densities are obtained for the given guiding center density by distributing the particles along their appropriate circular orbits as already described.

If the initial distribution of any of the species is uniform, it will remain so also at later times due to the incompressibility of the flow. Initial conditions where only the electron component is perturbed will therefore be unaffected by FLR effects and the time variation of the electric field will be similar to the one described by e.g., Seyler *et al.* [1].

In dimensionless units the governing equations, with the FLR corrections incorporated, take the form

$$\frac{\partial n_i}{\partial t}+\nabla\cdot(n_i\overline{\boldsymbol{v}})=0, \tag{7}$$

$$\frac{\partial n_e}{\partial t}+\nabla\cdot(n_e\boldsymbol{v})=0, \tag{8}$$

$$\boldsymbol{v}=-\nabla\Phi\times\boldsymbol{b}, \tag{9}$$

$$\nabla^2\Phi=-(\overline{n_i}-n_e), \tag{10}$$

where $\overline{\boldsymbol{v}}$ and $\overline{n}$ are obtained from Eqs. (5) and (6), respectively. Again it should be stressed that n_e and n_i are the electron and ion guiding center densities, respectively. A typical simulation of the potential evolution is shown in Fig. 1.

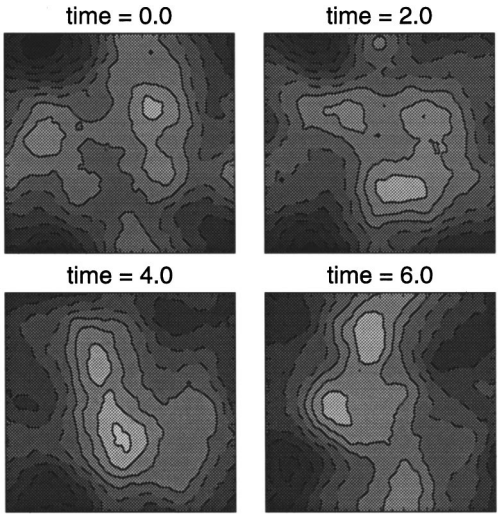

FIG. 1. The time evolution of the potential in a simulation with one electron and one ion species, where $\rho=0.5$ and the spatial dimension is $[0,10\rangle^2$ in dimensionless computational units. The solid contours indicate a positive potential, while the dashed contours correspond to a negative potential.

In the derivation of the governing equations (7)–(10), it was implicitly assumed that all the ions had the same Larmor radius. This constraint may be relaxed by averaging the ion velocity, or equivalently the ion Larmor radius, over a Maxwellian velocity distribution. Thus the averaged filter coefficient becomes $\hat{g}_{\boldsymbol{k}}=\exp[-(\rho k)^2/4]$. Effectively, this model assumes that the relative distribution of ion Larmor radii remains the same in a fluid element during its propagation and deformation. This assumption may be difficult to justify for a collisionless plasma.

Alternatively, we may construct a hybrid model consisting of many ion species, each characterized by their respective Larmor radius ρ. The electrons still obey the continuity equation (8), while each ion species follows a continuity equation

$$\frac{\partial n_\rho}{\partial t}+\nabla\cdot(n_\rho\overline{\boldsymbol{v}_\rho})=0. \tag{11}$$

In addition, the Poisson equation must be modified to include the charge contributions from each ion species,

$$\nabla^2\Phi=\left(n_e-\sum_\rho\ \overline{n_\rho}\right). \tag{12}$$

First we demonstrate the results from a simulation where all the ions are assumed to have the same Larmor radius. Next, we include several ion components, with different Larmor radii, which interact through the collective electric field. As mentioned, consistency with the derivation of the basic equations, where polarization drifts were ignored, requires ρ to be much smaller than the scales characterizing the fluctuations and the size of the system. However, in the following we relax this condition somewhat in order to bring out the basic features more clearly.

III. NUMERICAL CONSIDERATIONS

The system of equations (7)–(10) is solved on a square grid with spatial dimensions $[0,L\rangle^2$ in dimensionless computational units. In the present simulations we used N^2 gridpoints with $N=128$. The parameters L and N are chosen independently. To approximate the spatial derivatives we employed a standard Fourier collocation scheme [8,9], with isotropic zero padding to avoid aliasing errors from the nonlinear products. Here all wave numbers where $|\boldsymbol{k}|\geqslant 2k_m/3$, with $k_m=2\pi N/(2L)$, are zero padded. The Fourier collocation scheme enforces periodic boundary conditions. Although inclusion of a large number of ion species in the extended system will give a time consuming code, a moderate number is acceptable on a parallel machine. Therefore the equations were implemented on an IBM-SP2 with 16 nodes. Each fluid is then assigned to a node and communicates with the master node at every time step in order to update the electrostatic potential.

To integrate the system of equations (7)–(10) in time, we used a fourth order Runge-Kutta method for the first two time steps. Then, we applied a partially corrected third order Adams-Bashforth method [10]. Here, the solution of an ordinary differential equation in the form

$$\frac{\partial C}{\partial t}=F(C) \tag{13}$$

is advanced in time by

$$\widetilde{C}^{n+1}=C^n+\frac{\Delta t}{12}\{23F^n-16F^{n-1}+5F^{n-2}\},$$

$$C^{n+1}=C^n+\frac{\Delta t}{12}\{5\widetilde{F}^{n+1}+8F^n-F^{n-1}\},$$

where $\widetilde{F}^{n+1}=F(\widetilde{C}^{n+1})$. The variables F^{n-2}, F^{n-1}, and F^n are subsequently updated to reflect the new time step. The partially corrected method replaces F^{n+1} with $\widetilde{F}^{n+1}$. Thus we are left with only one evaluation of the time consuming spatial operator, per time step.

The time step is chosen in accordance with the Courant-Friedrich-Levy condition [9]. This requires the time step to be smaller than the time a perturbation needs to propagate from one gridpoint to another. In the present simulations a characteristic velocity is $O(1)$ while the gridpoint spacing is $O(N^{-1})$. Hence the time step is chosen to be $\Delta t\lesssim 1/N$.

From the simulations of the Eulerian flow, we have access to the Eulerian velocity field at each time step. This is subsequently used to trace the position of a test particle simply by integration of its Lagrangian velocity, $\boldsymbol{r}(t)=\int_{t_0}^{t}\boldsymbol{v}(\boldsymbol{r}(\tau),\tau)\ d\tau$. Numerically this is done by a second order Runge-Kutta method,

$$\widetilde{\boldsymbol{r}}^{n+1}=\boldsymbol{r}^n+\Delta t\ \boldsymbol{v}(\boldsymbol{r}^n,n\Delta t),$$

$$\boldsymbol{r}^{n+1}=\boldsymbol{r}^n+\frac{1}{2}\Delta t\{\boldsymbol{v}(\boldsymbol{r}^n,n\Delta t)+\boldsymbol{v}(\widetilde{\mathbf{r}}^{n+1},(n+1)\Delta t)\}.$$

In addition, we must interpolate the Eulerian velocity field at the actual position of the test particle. Thus we have three

possible origins of error for tracking the particle. Results by Ramsden and Holloway [11] indicate that the choice of interpolation method (and integration method for the position), is basically unimportant compared to errors due to the finite resolution of the two-dimensional (2D) Eulerian dynamics. Fourier interpolation is discarded because of large computational expenses, $O(MN^2)$ where M is the number of test particles. Hence we choose bicubic splines in order to interpolate the velocity. This method has proven to be both accurate and fast [12], implying $O(N^2)$ operations for construction of the spline and $O(M)$ for evaluation. In the simulations we used $M=1225$ particles, which initially were distributed on $[0,L\rangle^2$, with uniform spacing. Test particles crossing a boundary are reintroduced at the corresponding position at the opposite boundary and the trajectory is continued. The system size L is added when calculating the net particle displacement. The particle tracking thus explicitly makes use of the periodicity of the system.

IV. EQUILIBRIUM SPECTRA

With the FLR corrections given by the foregoing arguments, Knorr and Pécseli [13] worked out an analytical expression for the spectral equilibrium distribution in the case of electrons and one ion species. We use these results as a test of our program, but as they have not been investigated numerically before, the results are interesting by themselves.

In wave number space the equations (7)–(10) are given by their truncated Fourier representation

$$\frac{dn_{i\boldsymbol{k}}}{dt}=-i\boldsymbol{k}\cdot\sum_{\boldsymbol{p}+q=k}^{\boldsymbol{k}_{\max}} n_{i\boldsymbol{p}}\,\overline{\boldsymbol{v}_{\boldsymbol{q}}}, \tag{14}$$

$$\frac{dn_{e\boldsymbol{k}}}{dt}=-i\boldsymbol{k}\cdot\sum_{\boldsymbol{p}+\boldsymbol{q}=\boldsymbol{k}}^{\boldsymbol{k}_{\max}} n_{e\boldsymbol{p}}\,\boldsymbol{v}_{\boldsymbol{q}}, \tag{15}$$

$$\boldsymbol{v}_{\boldsymbol{k}}=-i\Phi_{\boldsymbol{k}}\,\boldsymbol{k}\times\boldsymbol{b}, \tag{16}$$

$$\Phi_{\boldsymbol{k}}=(\overline{n_{i\boldsymbol{k}}}-n_{e\boldsymbol{k}})/k^2, \tag{17}$$

where $\bar{\boldsymbol{v}}_{\boldsymbol{k}}=g_{\boldsymbol{k}}\boldsymbol{v}_{\boldsymbol{k}}$ and $\overline{n_{i\boldsymbol{k}}}=g_{\boldsymbol{k}}n_{i\boldsymbol{k}}$.

This truncated system possesses three invariants, the enstrophy for each species and the total energy. These are conserved quantities even for a finite number of wave numbers [13]

$$\Omega_{e,i}=\sum_{\boldsymbol{k}_0}^{\boldsymbol{k}_{\max}}|n_{e,i\boldsymbol{k}}|^2, \tag{18}$$

$$\mathcal{E}=\sum_{\boldsymbol{k}_0}^{\boldsymbol{k}_{\max}}|\overline{n_{i\boldsymbol{k}}}-n_{e\boldsymbol{k}}|^2/k^2. \tag{19}$$

By considering a microcanonical ensemble of systems consisting of the Fourier coefficients of n_e and n_i, evolving on the intersection of the hypersurfaces defined by (18) and (19), the equilibrium is given by the Boltzmann-Gibbs distribution

$$P(n_{e\boldsymbol{k}_1},\ldots,n_{e\boldsymbol{k}_{\max}},n_{i\boldsymbol{k}_1},\ldots,n_{i\boldsymbol{k}_{\max}})=\frac{1}{Z}\exp(-\mu_e\Omega_e-\mu_i\Omega_i-\beta\mathcal{E}), \tag{20}$$

where Z is the partition function

$$Z=\int e^{(-\mu_e\Omega_e-\mu_i\Omega_i-\beta\mathcal{E})}\prod_{\boldsymbol{k}_0}^{\boldsymbol{k}_{\max}} dn^r_{e\boldsymbol{k}}\,dn^i_{e\boldsymbol{k}}dn^r_{i\boldsymbol{k}}\,dn^i_{i\boldsymbol{k}}$$
$$=\prod_{\boldsymbol{k}_0}^{\boldsymbol{k}_{\max}}\left[\mu_i\mu_e+\frac{\beta}{k^2}(\mu_i+g^2_{\boldsymbol{k}}\mu_e)\right].$$

The superscripts r and i denote the real and imaginary parts, respectively. The distribution in (20) is characterized by the inverse ''temperatures'' μ_e, μ_i, and β corresponding to the fluctuations in n_e, n_i, and the total energy. Setting $Z=\Pi_{\boldsymbol{k}}Z_{\boldsymbol{k}}$ and differentiating the logarithm of the partition function $Z_{\boldsymbol{k}}$, with respect to these temperatures, the Fourier components of the spectral energy distribution

$$\langle\mathcal{E}_{\boldsymbol{k}}\rangle=\frac{1}{\beta+c^2_{\boldsymbol{k}}k^2},\quad\text{with}\quad c^2_{\boldsymbol{k}}=\frac{1}{\mu_e^{-1}+g^2_{\boldsymbol{k}}\mu_i^{-1}},$$

and the Fourier components of the electron and ion guiding center density

$$\langle|n_{e\boldsymbol{k}}|^2\rangle=\mu_e^{-1}\left(1-\frac{\beta c^2_{\boldsymbol{k}}\mu_e^{-1}}{\beta+c^2_{\boldsymbol{k}}k^2}\right),$$

$$\langle|n_{i\boldsymbol{k}}|^2\rangle=\mu_i^{-1}\left(1-\frac{\beta c^2_{\boldsymbol{k}}g^2_{\boldsymbol{k}}\mu_i^{-1}}{\beta+c^2_{\boldsymbol{k}}k^2}\right)$$

are found. With $\mu_e=1.0$, $\mu_i=0.1$, and $\beta=-9\times10^{-3}$, these expectation values are used as initial conditions for the simulations running for 4×10^4 time steps. The equilibrium state given by the negative temperatures is only possible for a finite system where $k_0=2\pi/L$ is nonzero [14]. The negative temperature state corresponds to a condensation of energy in the lowest k modes. However, no singularity arises in the spectrum, for small negative β values, because only discrete wave numbers enter the analysis. The spectrum is positive definite for all $|\boldsymbol{k}|>0$, and $|\boldsymbol{k}|=0$ does not enter the dynamical evolution.

In the limiting case of zero Larmor radius, where $g^2_{\boldsymbol{k}}=1$, the spectral energy distribution is characterized by β and an effective temperature $c^2_{\boldsymbol{k}}=\mu_e\mu_i/(\mu_e+\mu_i)$, independent of $\boldsymbol{k}$. It is easily shown that this limit reproduces the results of Seyler *et al.* [1], as expected. As mentioned earlier, the basic governing equations remain well behaved also in the formal limit $\rho\to\infty$, which, however, is violating the assumptions in the derivation. We note here that also the equilibrium spectra are well behaved in this formal limit, giving $g^2_{\boldsymbol{k}}=0$ and $c_{\boldsymbol{k}}=\mu_e$. A similar result is also obtained with $\mu_i^{-1}=0$. In these cases the ion motion is completely decoupled from the dynamics in our equations, while in the zero Larmor radius case the ion and electron dynamics are indistinguishable.

In Fig. 2, the time averaged, numerically obtained spectral distribution is compared with the theoretical result for two different ion Larmor radii. For simplicity we represent the

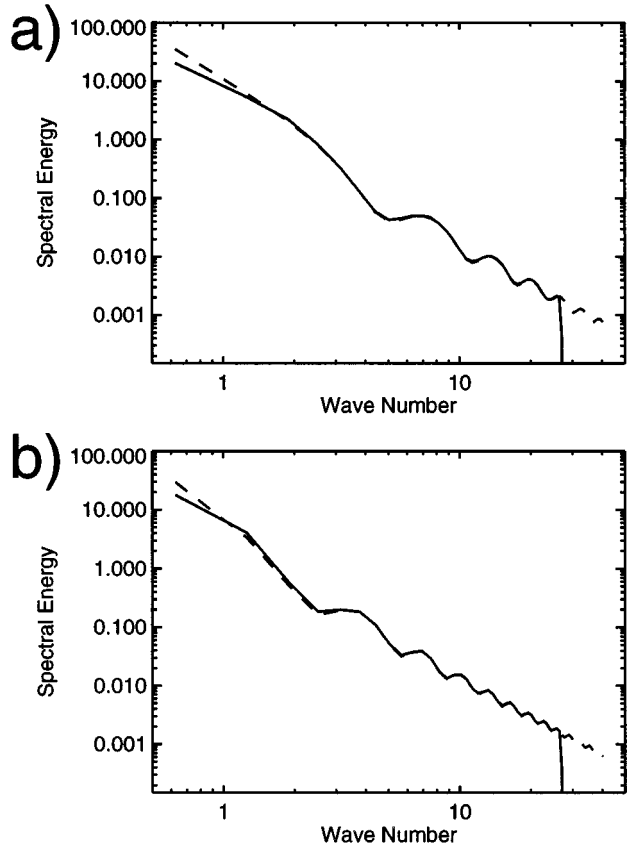

FIG. 2. Time averaged numerically calculated spectrum (solid line) compared to the analytical result (dashed line) for (a) $\rho=0.5$ and (b) $\rho=1.0$. The values of ρ are given in computational dimensionless units, where the simulated domain is $[0,10\rangle^2$. The abrupt drop in energy for large k is due to the zero padding scheme employed in the simulations.

spectra by continuous curves, even though the analysis as well as the simulations refer to discrete wave numbers. In particular, Fig. 2(a) corresponds to the potential evolution shown in Fig. 1. The spectra are obtained as a time average over the entire simulation. Alternatively, the spectra can be obtained at a selected time step or as an average over a reduced time interval, at the expense of an increased uncertainty, giving rise to some irregularity in the spectral shape. Apart from this statistical scatter, the results in Fig. 2 are representative for selected wave number spectra during the entire calculation. The dynamics in configuration space are thus highly dynamic, see Fig. 1, while the power spectrum is essentially stationary, as expected. The stability of the spectra was explicitly verified by demonstrating the relaxation of a perturbed spectrum towards the theoretical distribution of energy in wave number space. In this case, the equilibrium spectra were perturbed by increasing the energy in a few central wave numbers by an order of magnitude. Alternatively, we have observed the relaxation from an initial condition where energy was concentrated in a ring in wave number space, but this relaxation took a noticeably longer time.

The agreement between the numerical results and the theoretical prediction is good, indicating that the results quoted above represent the correct wave number spectral distributions. In particular, it can be argued that Ω_e, Ω_i, and

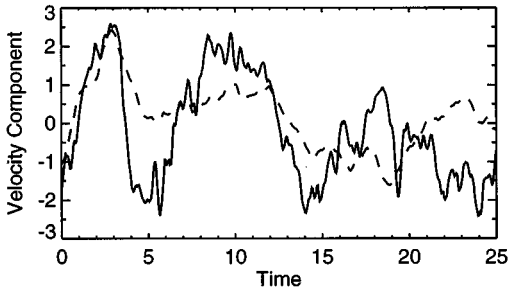

FIG. 3. The Lagrangian velocity components (x direction) for a typical electron (solid line) and ion (dashed line) test particle where $\rho=0.5$.

$\mathcal{E}$ are the *only* invariants of the truncated system (14)–(17). If the analytical results of Knorr and Pécseli [13] are accepted *a priori*, the results of Figs. 2(a) and 2(b) serve on the other hand as a test of the accuracy of the code. The only conspicuous deviations between the analytical results and the simulations are for the smallest wave numbers in the system.

V. TURBULENT DIFFUSION

The finite Larmor radius effects discussed in the foregoing section will be particularly important for low-frequency electrostatic turbulence in strongly magnetized plasmas. Here electrons and ions diffuse at different rates because of the difference in the $\boldsymbol{E}\times\boldsymbol{B}$ drifts they experience in the same turbulent electric field. In order to demonstrate the basic features of this process we used the code discussed in the foregoing section to analyze the consequences of the FLR corrections for turbulent transport. In order to study well defined conditions, we assume the equilibrium spectra discussed in Sec. IV.

The most important quantity for describing the diffusion in the present context is the normalized Lagrangian velocity autocorrelation function

$$R(s)=\frac{\langle \boldsymbol{V}(t)\cdot\boldsymbol{V}(t+s)\rangle}{\langle V^2\rangle}, \tag{21}$$

with $\boldsymbol{V}(t)=\mathbf{v}(\mathbf{r}(t),t)$. For homogeneous and time stationary turbulence, $R(s)$ contains all relevant information necessary for obtaining the mean-square particle displacement $\langle r^2(t)\rangle$. Thus it is well known [15] that

$$\langle r^2\rangle=2\langle V^2\rangle t\int_0^t(1-s/t)R(s)ds.$$

This expression can be approximated for both small and large t,

$$\langle r^2\rangle\approx\begin{cases}\langle V^2\rangle t^2, & t\ll\lambda\\ 2\langle V^2\rangle\tau t, & t\gg\tau.\end{cases} \tag{22}$$

For large times, $t\gg\tau$, this corresponds to the diffusive limit, where the integral time scale is $\tau\equiv\int_0^\infty R(s)ds$. For small times, $t\ll\lambda$, we have the convective regime, where λ is the micro time scale [16] defined as $\lambda=\sqrt{-2/R''(0)}$. The relation between the Lagrangian and the Eulerian velocity auto-

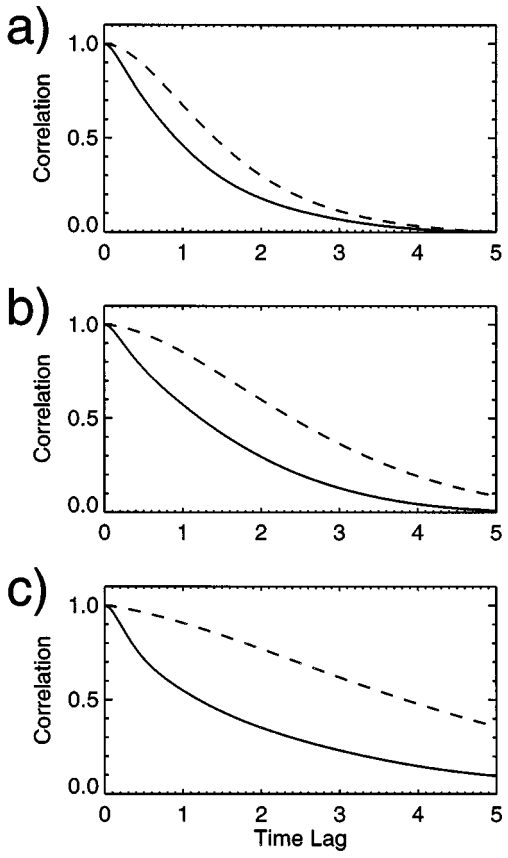

FIG. 4. Lagrangian velocity autocorrelation functions for electrons (solid line) and ions (dashed line) obtained from simulations with *one* ion species in addition to the electrons. The results are shown for three different ion Larmor radii, $\rho=0.5$, 1.0, and 1.5, corresponding to (a), (b), and (c), respectively. The figure is obtained by tracking 1225 test particles for 4×10^4 time steps corresponding to 100 dimensionless computational time units.

correlation functions has been discussed in detail by Pécseli and Trulsen [17]. However, they used a different model, where the flow consisted of many point vortices convected by their mutual electrostatic field.

A. Flow with one ion component

With the flow fields being different for electrons and ions [even though they are derived from the same space-time varying electric field, see (5)], two different correlation functions can be defined; one for electrons and one for the ion species specified by the Larmor radius ρ. Consequently, each species has its own associated integral time scale, τ_e and τ_i; and similarly for the micro time scales, λ_e and λ_i.

As discussed in the foregoing section, the electric field power spectrum changes with the ion Larmor radii in the initial conditions. Given the spectrum of the fluctuations, the electrons experience the full energy in the electric field while the ions experience a field which is reduced by the $J_0(k\rho)$ factor in (5). This is readily observed in Fig. 3 where the x component of the Lagrangian velocity is shown for one electron and one ion test particle. Both were released at the *same* initial position, but their velocities rapidly become uncorrelated. Also, it is evident that the ion velocity variation is

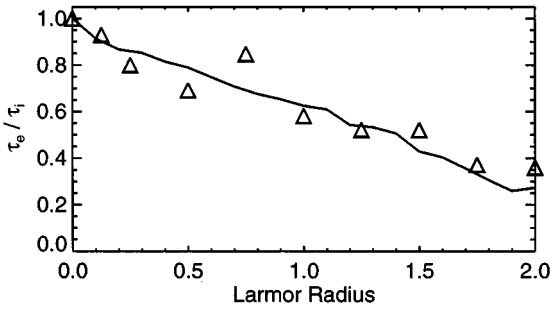

FIG. 5. The ratio τ_e/τ_i is shown as a function of ρ in dimensionless, computational, units. The solid line shows the analytical result, while triangles correspond to results obtained from direct numerical simulations. The analytical results are based on the actual spectra in the simulations. Since these are statistically fluctuating in individual realizations, the analytical curve exhibits corresponding irregularities.

smaller and smoother on the average compared to the electron velocity. The FLR corrections for the ion dynamics have the consequence that an initially close electron-ion gyro center pair will separate faster than in the zero Larmor radius case. Two initially close electrons will on the other hand remain close for an extended time since they experience essentially the same $\boldsymbol{E}\times\boldsymbol{B}$ flow, similarly for initially close ion gyro centers. The problem of relative diffusion [18] will be discussed in a different work.

A comparison between the electron and ion velocity correlation functions corresponding to the *same* flow clearly indicates an increase in the integral time scale τ_i for the ions for increasing ρ. Results are shown in Fig. 4 for $\rho=0.5$, 1.0, and 1.5 in computational dimensionless units. For $\rho=0$ the velocity statistics for the electrons and ions are the same and the autocorrelation functions are therefore identical. The results are readily understood by the difference in rms velocities for electrons, $\langle v_e^2\rangle=\int\mathcal{E}(k)d\boldsymbol{k}$, and for ions, $\langle v_i^2\rangle=\int\mathcal{E}(k)J_0^2(k\rho)d\boldsymbol{k}$. The mean-square velocity is larger for the electrons than for the ions since $J_0^2(k\rho)\leqslant1$. The integral time scale can be estimated by the ratio of a length scale which is determined by $\mathcal{E}(k)$ and a velocity $\langle v^2\rangle^{1/2}$. Since ions and electrons move in the same electric field spectrum, the characteristic length is the same for both species, while their rms velocities are different for different ρ by the arguments given before. By this heuristic argument we expect that the integral time scale increases for increasing Larmor radius. Hence the ratio τ_e/τ_i is estimated as

$$\frac{\tau_e}{\tau_i}=\sqrt{\frac{\langle v_i^2\rangle}{\langle v_e^2\rangle}}. \tag{23}$$

In Fig. 5 we show this quantity with a full line where $\langle v_{e,i}^2\rangle$ is obtained from the initial equilibrium spectrum. The ratios of the actual integral time scales obtained from the simulations are indicated by triangles. Considering the simplicity of the argument, the agreement is good. The small irregularities in the full line are caused by fluctuations in the simulation spectra.

The result (23) is expressed in terms of the integral time scales $\tau_{e,i}$ for electrons and FLR-corrected ions. These time

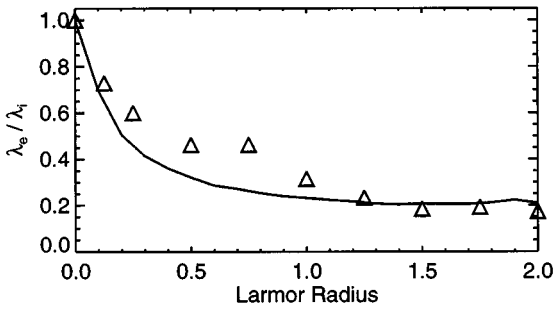

FIG. 6. The variation of the ratio λ_e/λ_i is shown for increasing ρ in dimensionless computational units. The solid line shows the analytical result, while the triangles correspond to results obtained from direct numerical simulations.

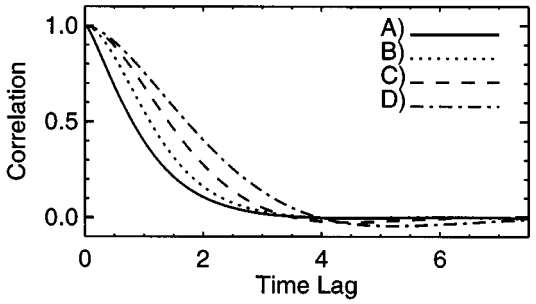

FIG. 7. Lagrangian velocity autocorrelation functions for a simulation containing electrons and three ion species with different Larmor radii. The solid line corresponds to the electrons, while (B), (C), and (D) correspond to ions with $\rho=0.5$, 1.0, and 1.5 respectively. Times are in dimensionless computational units.

scales are determined by the integral of the entire respective velocity correlation functions. Alternatively, a micro time scale λ is determined by the curvature of the respective correlation function at the origin, i.e., $\lambda=\sqrt{-2/R''(0)}$. Also this time scale is sensitive to FLR corrections. From Fig. 4 we notice that the curvature of $R(s)$ at $s=0$ decreases with increasing ρ, or equivalently that λ increases with increasing ρ. A graph of the ratio λ_e/λ_i as a function of ρ is shown in Fig. 6. The curvature of the correlation function at $s=0$ was determined by a parabolic fit. This figure is obtained from simulations with one electron and one ion species where ρ is varied systematically.

We can give analytical estimates for the ratio λ_e/λ_i by making use of the short time approximation of the Lagrangian autocorrelation function. For small t we may approximate the trajectory of the fluid element by a straight line $\boldsymbol{r}(t)=\boldsymbol{r}_0+\boldsymbol{u}t$ with constant $\boldsymbol{u}$, insert this approximation in (21), and average over a Maxwellian velocity distribution $P(\boldsymbol{u})$. In addition, we use that the Fourier transform of the autocorrelation function is given by the power spectrum. An approximation of the Lagrangian autocorrelation function, in terms of the Eulerian spectrum, is then obtained as

$$R(s)\approx\frac{1}{\langle u^2\rangle}\sum_{k_x}\sum_{k_y}\mathcal{E}(\boldsymbol{k})\exp\left[-\frac{s^2\langle u^2\rangle}{2}(k_x^2+k_y^2)\right]. \quad (24)$$

This approximation is based on an assumption of a frozen velocity field, in which a fluid element is convected without distortion. The approximation can be improved if the velocity entering the exponent in the Lagrangian autocorrelation function is replaced by the rms velocity of the particle and the velocity of the flow. The argument implies that the flow field in which a test particle propagates is distorted by motion of surrounding vorticity centers which have a velocity of the order of $\langle v_e\rangle^{1/2}$. Following, e.g., Wandel and Kofoed-Hansen [19] we then estimate the rms-difference velocity between a test particle and these vorticity centers as $(\langle v_e^2\rangle+\langle v_i^2\rangle)^{1/2}$ for an ion and $\sqrt{2}\langle v_e^2\rangle^{1/2}$ for an electron. These estimates are then used for $\langle u^2\rangle$ in (24), see also Landahl and Mollo-Christensen [16]. By a Taylor expansion of $R(s)$ around $s=0$, the ratio of λ_e/λ_i is then estimated as

$$\frac{\lambda_e}{\lambda_i}=\sqrt{\frac{\langle v_e^2\rangle+\langle v_i^2\rangle}{2\langle v_i^2\rangle}}\sqrt{\frac{\Sigma_{k_x}\Sigma_{k_y}J_0^2(\rho k)\mathcal{E}(\boldsymbol{k})k^2}{\Sigma_{k_x}\Sigma_{k_y}\mathcal{E}(\boldsymbol{k})k^2}}. \quad (25)$$

In Fig. 6 this ratio is compared with the numerically obtained results. Although there is some discrepancy between the theoretical and the numerically obtained results, the overall shape of the curve is reproduced by the theory. Obviously, the results agree exactly for $\rho=0$. The agreement of simple estimates such as (23) and (25) with the numerical results may seem surprising. It is, however, important that it is the *ratios* of characteristic quantities that are estimated and not quantities themselves. A common error in the coefficients of the relevant time scales will be canceled in (23) and (25). For practical applications it is the ratio of time scales which is most interesting and important, since it contains the information of the charge separation which depends on the FLR effects.

B. Flow with several ion components

As discussed in Sec. II, the system of equations (7)–(10) is easily extended to include the more realistic case where many different ion Larmor radii are simultaneously present in the flow. In this way a multifluid model is obtained where the relative density of the various ion components can be chosen according to an *a priori* given velocity distribution, e.g., a Maxwellian. This multifluid model will be characterized by different mobilities of the ion components in addition to ion-electron differences already discussed. In Fig. 7 we show as an illustration the Lagrangian velocity autocorrelation functions for the case where three ion components with different Larmor radii are simultaneously present in the same flow. Again we observe an increase in the integral time scale τ for increasing ρ, caused by the filtering of the spectrum by the J_0 function. The results are qualitatively consistent with those of Fig. 4, where only one ion species was present. We notice that the velocity correlation takes on negative values for large time separations.

In Fig. 8 we show the root-mean-square particle displacement (''absolute diffusion'') for a simulation identical to the one described in Fig. 7. As expected, the mean-square displacement is proportional to t in the convective regime and proportional to $\sqrt{t}$ in the diffusive limit, see (22). For clarity, two lines with slopes corresponding to t and $\sqrt{t}$ are included in the figure. Equally important is the fact that ion species with different Larmor radii, but present in the same flow,

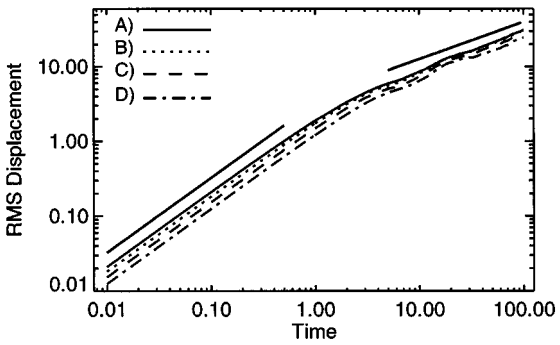

FIG. 8. Plot of the rms displacement of the test particles, (A) corresponds to the electrons while (B), (C), and (D) correspond to ions with increasing Larmor radius, $\rho = 0.5$, 1.0 and 1.5 respectively.

have different dispersion rates. From Fig. 8 it is evident that electrons, which experience the full energy in the electric field, have a larger mean-square displacement than the ions. In addition, the ion dispersion rate is seen to increase with the inverse Larmor radius, as expected. These differences in turbulent diffusion rates give rise to charge separation effects which are absent in the zero Larmor case.

VI. CONCLUSIONS

In this paper we presented an implementation of a computationally advantageous code for including finite Larmor radius effects in a fluid model. The problem was studied numerically by Knorr *et al.* [7], but in a formulation where they averaged over Larmor radii for ions having gyro centers in a small area of configuration space. Physically, this averaging, which leads to a particularly simple form of the convolution, assumes that all the ions in that small area follow essentially the same orbit. This can be achieved if there is a strong collisional interaction between the ions. The simplicity of the formalism used by Knorr *et al.* [7] was thus obtained at the expense of a somewhat uncertain physical model, which we avoided in the present study.

In addition to standard accuracy tests, equilibrium spectra obtained from direct numerical simulations of the equations (7)–(10) were compared to analytical results. Excellent agreement was found, adding confidence to our code and also to the theoretical analysis. These particular equilibrium spectra have not been studied numerically before. We applied the code for a study of turbulent transport, demonstrating that FLR effects have nontrivial effects on the dispersion of charged particles in magnetized plasmas. For turbulent, inhomogeneous plasmas this difference in diffusion rates will have significant influence on the buildup of ambipolar dc-electric fields, and subsequently also on the bulk flow characteristics. Even though the finite Larmor radius effects give small corrections to the $\boldsymbol{E}\times\boldsymbol{B}$ drift, these corrections have important consequences by giving rise to charge separation effects which are absent for vanishing FLR corrections. The analysis in this paper was based on a continuum model in two spatial dimensions. The effects considered here can, however, also be included in a generalized, discrete Hamiltonian vortex model as discussed in [13]. We have also studied this model, but the analysis falls outside the scope of this paper.

From the multifluid simulations we obtain results which qualitatively agree with expectations based on two-fluid simulations and a systematic variation of ρ. The Lagrangian velocity autocorrelation function experiences the same broadening as ρ increases in both the two-fluid and the multifluid simulations. The basic features of the rms displacement are also reproduced in the multifluid simulations.

When a density gradient is present, turbulent $\boldsymbol{E}\times\boldsymbol{B}$ diffusion of electrons and ions will necessarily be ambipolar due to the different diffusion rates of the various ion species present, caused by the finite Larmor radius effects. If locally homogeneous and isotropic conditions can be assumed, our results on characteristic time scales can be used to estimate the time for buildup of these ambipolar electric fields.

We have generalized our model and numerical code to the case where the electrons can be assumed to be in a local isothermal Boltzmann equilibrium, while a two-dimensional description is retained for the ions. These results will be presented in a different context.

ACKNOWLEDGMENTS

This work was supported in part by the Norwegian Research Council for Science and Humanities (NFR) and the program for supercomputing. One of us (B.K.) thanks ''Tungregneutvalget'' at NFR for providing computational time on the IBM cluster in Oslo.

[1] C. E. Seyler, Y. Salu, D. Montgomery, and G. Knorr, Phys. Fluids **18**, 803 (1975).
[2] P. M. Kintner and C. E. Seyler, Space Sci. Rev. **41**, 91 (1985).
[3] S. I. Braginskii, *Reviews of Plasma Physics* (Consultants Bureau, New York, 1965), Vol. 1.
[4] A. I. Smolyakov, I. O. Pogutse, and A. Hirose, Phys. Plasmas **2**, 4451 (1995).
[5] F. F. Chen, *Introduction to Plasma Physics and Controlled Fusion*, 2nd ed. (Plenum Press, New York, 1990).
[6] K. Stasiewicz, Space Sci. Rev. **65**, 221 (1994).
[7] G. Knorr *et al.*, Phys. Scr. **38**, 829 (1988).
[8] C. Canuto, A. Quarteroni, M. Y. Hussaini, and T. A. Zang, *Spectral Methods in Fluid Dynamics* (Springer-Verlag, Berlin, 1989).
[9] D. Gottlieb and S. A. Orszag, *Numerical Analysis of Spectral Methods; Theory and Applications* (SIAM, Philadelphia, 1977).
[10] J. Gazdag, J. Comput. Phys. **20**, 196 (1976).
[11] D. Ramsden and G. Holloway, J. Comput. Phys. **95**, 101 (1991).

[12] P. K. Yeung and S. B. Pope, J. Comput. Phys. **79**, 373 (1988).
[13] G. Knorr and H. L. Pécseli, J. Plasma Phys. **41**, 157 (1988).
[14] H. Kraichnan, J. Fluid Mech. **67**, 155 (1975).
[15] G. I. Taylor, Proc. London Math. Soc. **20**, 196 (1921).
[16] M. T. Landahl and E. Mollo-Christensen, *Turbulence and Random Processes in Fluid Mechanics*, 2nd ed. (Cambridge University Press, New York, 1992).
[17] H. L. Pécseli and J. Trulsen, J. Plasma Phys. **54**, 401 (1995).
[18] J. H. Misguich *et al.*, Plasma Phys. Contr. Fusion **29**, 825 (1987).
[19] C. F. Wandel and O. Kofoed-Hansen, J. Geophys. Res. **67**, 3089 (1962).